PAPER

Influence of repetition frequency on streamer-to-spark breakdown mechanism in transient spark discharge

IOP Publishing Journal of Physics D: Applied Physics

J. Phys. D: Appl. Phys. **50** (2017) 425207 (8pp) https://doi.org/10.1088/1361-6463/aa8940

Influence of repetition frequency on streamer-to-spark breakdown mechanism in transient spark discharge

M Janda[1], V Martišovitš[1], A Buček[1,2], K Hensel[1], M Molnár[1] and Z Machala[1]

[1] Faculty of Mathematics, Physics and Informatics, Comenius University Bratislava, Mlynská dolina, 842 48 Bratislava, Slovakia
[2] Faculty of Science, Masaryk University, Kotlářská 267/2, 611 37 Brno, Czechia

E-mail: janda@fmph.uniba.sk

Received 20 July 2017, revised 23 August 2017
Accepted for publication 30 August 2017
Published 27 September 2017

Abstract

Streamer-to-spark transition in a self-pulsing positive transient spark (TS) discharge was investigated at different repetition frequencies. The temporal evolution of the TS was recorded, showing the primary streamer and the secondary streamer phases. A streak camera-like images were obtained using spatio-temporal reconstruction of the discharge emission detected by a photomultiplier tube with light collection system placed on a micrometric translation stage. With increasing TS repetition frequency f (from ~1 to 6 kHz), the increase of the propagation velocity of both the primary and the secondary streamer was observed. Acceleration of the primary and secondary streamers, and shortening of streamer-to-spark transition time τ with increasing f was attributed to the memory effect composed of pre-heating and gas composition changes induced by the previous TS pulses. Fast propagation of the secondary streamer through the entire gap and fast gas heating could explain the short τ (~100 ns) at f above ~3 kHz.

Keywords: streamer breakdown, secondary streamer, spatio-temporal optical diagnostics, transient spark

(Some figures may appear in colour only in the online journal)

1. Introduction

Streamer-to-spark transition leading to the gas breakdown is a critical issue when working with atmospheric pressure electrical discharges, as well as in the design of high voltage (HV) devices and switches. The gas breakdown and the spark formation are usually not desired. On the other hand, periodic streamer-to-spark transition with restricted spark phase can bring multiple benefits in various applications of non-thermal plasmas, such as local and transient elevation of the gas temperature, formation of hydrodynamic expansion, production of reactive species with high concentration, etc [1–5].

The first studies of the atmospheric pressure air breakdown mechanism appeared several decades ago [6–8] and the streamer breakdown theory was introduced by Meek [9], Raether [10] and Loeb [11] in the middle of the 20th century. However, because of the complexity of this problem, investigations of the breakdown mechanism, streamers and their propagation have continued through extensive studies of Marode *et al* in the 1970s–1980s [12–14] to the present [1, 15–18]. Various non-invasive optical diagnostic methods are commonly used to investigate fast transient discharge phenomena, such as streamers. A review on this topic was recently written by Šimek [19].

Fast changes of plasma properties in streamers imply high demands on their diagnostic methods. Time-resolved techniques with time resolution in the order of 1 ns (or better) must be used. This can be accomplished by using intensified high speed CCD cameras [3, 20–24]. In order to achieve high spatial resolution, iCCD microscopy technique can be employed [25–27].

The optical emission spectroscopy (OES) technique can provide valuable information on excited atomic and molecular states. It enables one to determine the rotational, vibrational and electronic excitation temperatures of the plasma and thus the level of non-equilibrium and gas temperature [28, 29]. It was also successfully applied for the time evolution of rotational temperature T_r from the primary streamer to the secondary streamer, using the second positive system of nitrogen [30]. The OES technique can be used to measure the electron density in the plasma as well. A review on this topic was recently written by Ivkovic *et al* [31].

The time-resolved imaging can also provide information about various streamer characteristics, such as propagation velocity, branching, or channel thickness [22, 23, 32]. The propagation of a single discharge event can be tracked using several synchronized iCCD cameras [22]. Fast streak cameras and cross-correlation spectroscopy (CCS) may also provide valuable information about the evolution of transient discharge events [33–35]. The CCS technique enables to detect the spatio-temporally resolved single microdischarge development, even though it is occurring statistically [33]. The CCS technique was also recently used for the visualization of the streamer-to-spark transition in the transient spark (TS) [36].

Transient spark (TS), similar to previously reported prevented spark by Marode [37], is a dc-driven self-pulsing discharge with the typical repetition frequency 1–10 kHz [5, 38, 39]. Plasma generated during the TS spark phase is highly reactive, since the electron density as high as 10^{17} cm^{-3} can be achieved [40]. As a result, the TS have already been successfully demonstrated for disinfection/sterilization or flue gas cleaning in biomedical and environmental applications, respectively [41–43]. Fundamental research of the TS characteristics has been performed [5, 38, 39, 44, 45]. However, further studies are needed to explain changes of the TS characteristics and breakdown mechanism with increasing repetition frequency [38, 39].

The advanced CCS technique enabled us to study the TS discharge only at repetition frequency 8–10 kHz, where a very fast streamer-to-spark transition within ~10 ns was observed [36]. This was attributed to memory effects (pre-heating and gas composition changes induced by the previous TS pulses) leading to a low net electron attachment rate and acceleration of step-wise ionization processes. The objective of this paper is to investigate the changes of the streamer-to-spark transition mechanism leading to the spark breakdown in the air TS at repetition frequency below 8 kHz. The comparison of streamer-to-spark transition at different frequencies can help us to identify individual processes influencing streamer breakdown mechanism and how their roles change with increasing spark pulse repetition rate.

For this purpose we performed time resolved emission spectroscopy of the TS discharge streamer-to-spark transition phase using a fast iCCD camera coupled with a spectrograph. Next, the spatio-temporally resolved evolution of the primary and the secondary streamers in the TS was obtained by a photomultiplier tube (PMT), with the light collection system set on a micrometric translation stage. Processing of the PMT signals recorded at various positions in the gap enabled us to reconstruct the propagation of the primary streamer, secondary streamer and spark, with the visual output similar to a streak camera or the CCS technique.

2. Experimental setup

The TS is typically generated in atmospheric pressure air or other gases between metal electrodes in point-to-plane configuration with distance $d = 4$–10 mm, by a DC HV power supply connected to the electrodes via a series resistor $R = 5$–10 MΩ (figure 1(a)). Both polarities are possible; here we present a study of positive polarity TS discharge with stainless steel anode as the HV point electrode. An additional small resistor $r = 1$ kΩ was attached directly to the anode to eliminate oscillations of electric signals caused by the internal inductance of the HV cable connecting the resistor R and the anode. More details about the role of r on TS characteristics are provided in [38].

The discharge voltage was measured by an HV probe *Tektronix P6015A* and the discharge current was measured on a 50 Ω or 1 Ω resistor shunt. The 1 Ω resistor shunt was used for the TS spark current pulse, whereas the 50 Ω resistor shunt enabled us to measure streamer current pulses with higher sensitivity. Both voltage and current signals were recorded by a 200 MHz digitizing oscilloscope *Tektronix TDS2024*.

The time-resolved spectra were acquired using the an intensified CCD camera *Andor Istar* (2 ns minimum gate) coupled to a 2 m spectrograph *Carl Zeiss Jena PGS2* (spectral resolution 0.04–0.09 nm depending on the entrance slit width), covering the UV and VIS regions (200–800 nm). We used the emission spectra of the 0–0 band of the N_2 second positive system at 337 nm for the calculation of time-resolved rotational temperature T_r of the $N_2(C)$ species. The T_r was obtained by fitting the experimental spectra with the simulated ones using the *Specair* program [28]. We further used T_r as an indicator of the gas temperature T_g.

Time-resolved spectroscopy requires good synchronization of discharge electrical signal and light signal detection. Since the TS is a self-pulsing discharge, the synchronization between TS current pulses and the iCCD camera cannot be provided by an external trigger generator. Instead, the current signal of the TS itself was used to trigger the acquisition of the optical signal. The measurement of the discharge current on the shunts enabled us to synchronize the acquisition of the emission either with the beginning of the streamer (50 Ω shunt), or with the beginning of the spark (1 Ω shunt). As the current pulse reached a specified value, a TTL trigger generator sent a voltage pulse to the iCCD camera to initiate the light acquisition. The drawback of this approach is a delay (~45 or 55 ns, depending on the camera settings), caused by the TTL trigger generator, the transmission time of the signal through BNC cables, and the camera insertion delay. This delay was compensated in a large 2 m spectrograph (PGS-2) and by using a 10 m long optical fiber *Ocean Optics P400-10-UV–VIS,* so that photons travel ~75 ns before they reach the iCCD camera (see in figure 1(b)), to make sure the camera can detects them.

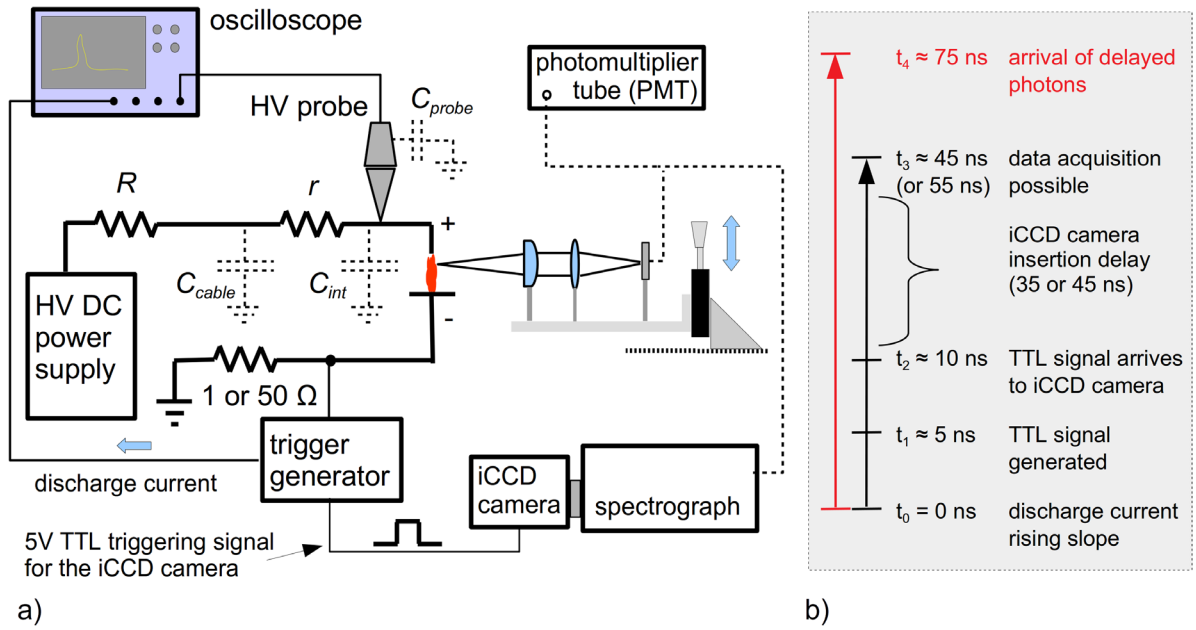

Figure 1. Schematic of the experimental setup (a), including the timing diagram explaining synchronization of the iCCD camera with the TS discharge (b): t_0—discharge current rising slope, t_1—generation of 5 V TTL signal for the iCCD camera, t_2—TTL signal reaches the iCCD camera (~5 ns delay caused by 1 m BNC cable), t_3—earliest possible data acquisition by the iCCD camera due to iCCD insertion delay, t_4—photons generated in t_0 reach the iCCD camera (delayed by traveling 10 m in the optical fiber and 8 m inside the spectrograph).

The spatio-temporal evolution of the discharges was analyzed by a PMT *Hamamatsu H955*. The light collection system was set on a micrometric translation stage to enable mapping of the light emission along the electrode's axis (0.5 mm spatial resolution). A cylindrical lens was used in the optical system to collect all the light in the plane perpendicular to the electrode's axis to avoid missing any discharge channel in case of its off-axis propagation. In order to isolate the N_2 (C–B, 0–0) transition for PMT measurements, a bandpass interference filter *Melles Griot 03 FIU127* was inserted into the optical path. The PMT module signal was recorded using the oscilloscope. The waveforms of the discharge current and PMT signal, averaged over 128 individual discharges, were recorded by the oscilloscope and subsequently processed and visualized. Processing of the PMT signals in the gap space and in time (2 ns resolution) enabled us to reconstruct the propagation of the primary streamer, secondary streamer and spark, with the visual output equivalent to a streak camera.

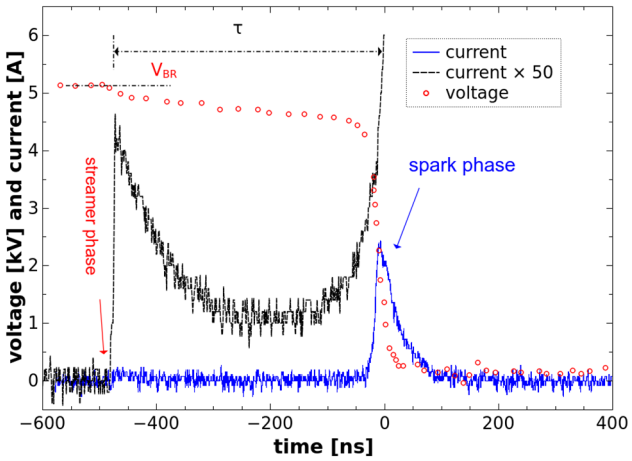

Figure 2. Typical waveforms of TS discharge, $f \sim 3.5$ kHz, $d = 4.5$ mm, $C \sim 24$ pF, $R = 6.5$ MΩ, $r = 1$ kΩ.

3. Results and discussion

The TS is initiated by a primary streamer (streamer phase) creating a relatively conductive plasma bridge between the electrodes. It enables partial discharging of the internal capacity C of the electric circuit (composed of internal capacity of the discharge chamber C_{int}, capacity of the HV cable C_{cable} between the ballast resistor R and the anode, and capacity of the HV probe $C_{probe} = 3$ pF), and a local gas heating inside the plasma channel [39]. When the gas temperature T inside the plasma channel reaches ~1000 K, a very short (~10–100 ns) high current (>1 A) spark current pulse appears (figure 2).

During the spark phase that lasts only a few tens of nanoseconds, the internal circuit capacity C completely discharges, and the potential V on the HV electrode drops to almost zero. Transition to steady-state arc after the spark is restricted by the ballast resistor R, and the discharge starts to decay after the voltage drop. Eventually, the potential V starts to gradually increase as the capacity C recharges. A new TS pulse, initiated by a new primary streamer, occurs when V reaches the breakdown voltage V_{BR} again. The TS is thus based on the repetitive primary streamer formation transiting to the spark, with the frequency f in the kHz range.

The increase of the TS repetition frequency f influences various discharge characteristics, including the breakdown mechanism [38, 39]. The decrease of the breakdown voltage and shortening of the streamer-to-spark transition time (τ) were observed with increasing f (figure 3). At ~8–10 kHz, the transition from the streamer to the spark proceeds very fast within about 10 ns [36], while at ~1 kHz the streamer-to-spark

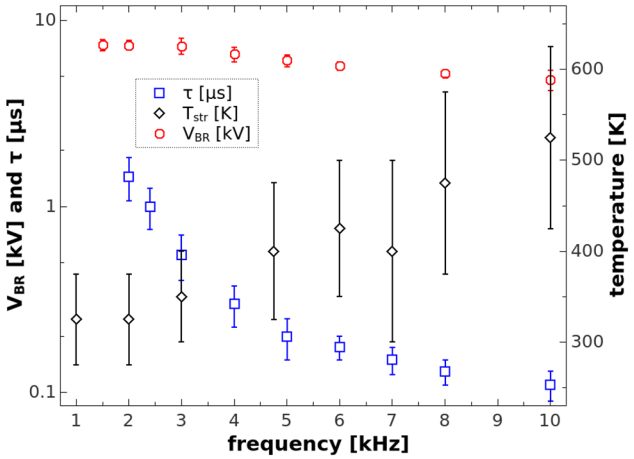

Figure 3. Breakdown voltage V_{BR}, average streamer-to-spark transition time τ and temperature T_{str} at the beginning of the streamer phase of the TS as functions of the repetition frequency, $R = 8.2\ \mathrm{M\Omega}$, $r = 1\ \mathrm{k\Omega}$, $C \approx 32$ pF, $d = 5$ mm. The temperature was measured as the rotational temperature of $N_2(C)$ species near the anode during the initial 5–20 ns of the streamer.

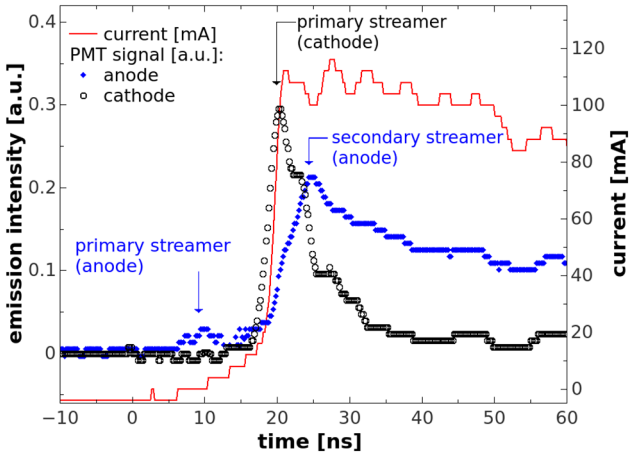

Figure 4. PMT signals of the TS discharge (streamer phase) measured near the anode and the cathode, respectively, synchronized with the discharge current measured on the 50 Ω shunt, $f \approx 1$ kHz, $d = 7$ mm.

transition time can exceed 1 μs. The decrease of V_{BR} with growing f can be explained by the increase of temperature measured near the anode at the beginning of the TS streamer phase, T_{str}. At higher temperatures, lower V_{BR} is required to keep E/N constant, thanks to the decrease in N resulting from the increase in the gas temperature. Based on the CCS measurements at $f \sim 10$ kHz, the shortening of τ was attributed to memory effects, leading to a low net electron attachment rate [36]. In order to verify this hypothesis, we studied the streamer-to-spark transition at lower frequencies.

For this purpose we used PMT with the light collection system placed on micro-metric translation stage. We measured simultaneously the discharge current on 50 Ω shunt. Thus, we were able to collect light from different positions in the gap and to synchronize them by the streamer current pulse (figure 4). The mapping of the light emission along the electrode's axis (spatial resolution 0.5 mm) enabled us to construct streak camera-like images of the TS discharge spatio-temporal evolution (figures 5 and 6) in a similar concept as in [12]. These images enabled us to identify two events, identified as the primary and the secondary streamer.

The name '*secondary streamer*' was first used by Loeb who suggested it was a new ionization wave [11], but according to Bastien and Marode, it is governed by attachment processes [14]; more precisely, by the distribution of the attachment rate along the plasma filament generated by the primary streamer. Higher attachment rate leads to the faster decrease of the electron density. This is equivalent to the decrease of the plasma conductivity and results in the reduced electric field E/N increase near the anode [14, 46–48]. The E/N near the anode can be as high as ~80 Td [47]. This is high enough for the generation of excited N_2 species emitting photons, observed as 'the secondary streamer'.

Axial emission intensity distribution of the primary streamer (figure 7) supports the existence of the non-homogeneous axial E/N distribution. The primary streamer emission intensity increases with the distance from the anode. According to the PMT signal measured with and without the interference filter, the majority of the primary streamer emission can be attributed to the $N_2(C)$–$N_2(B)$ radiative transition. The $N_2(C)$ excited states are mostly generated by the direct electron impact excitation of the ground state molecular nitrogen [49]. The increase of the emission intensity closer to the cathode thus indicates a non-homogeneous distribution of electron density along the filament, with increasing n_e towards the cathode. The conductivity σ of weakly ionized plasma is proportional to the electron density, and the current density $j = \sigma E$. As a result, the axial distribution of the electric field must be non-homogeneous after the primary streamer bridges the gap, with higher E near the anode.

The streak camera-like images of the TS discharge spatio-temporal evolution (figures 5 and 6) also enabled us to determine the primary and the secondary streamer velocities at different TS frequencies (figure 8), including their evolution along the gap. The average velocity was estimated from the time the primary and the secondary streamer needed to propagate through the entire gap, while the initial velocity was estimated from the time needed to propagate to the distance ~2.5 mm from the anode.

We observed that the primary streamer accelerates as it approaches the cathode, but the secondary streamer slows down. The velocities of both primary and secondary streamers increase with TS repetition frequency f (figure 8), but even at the lowest frequencies, the initial velocity of the secondary streamer is relatively high. The major difference was found below ~3 kHz: the secondary streamer does not propagate through the whole gap (figure 5). We thus assume that it is possible to divide the evolution of the secondary streamer into two phases: formation and propagation. The fast initial formation phase, which appears at all TS frequencies, is due to non-homogeneous axial conductivity distribution in the channel generated by the primary streamer. The following slower propagation phase occurs only under certain circumstances (at $f > 3$ kHz).

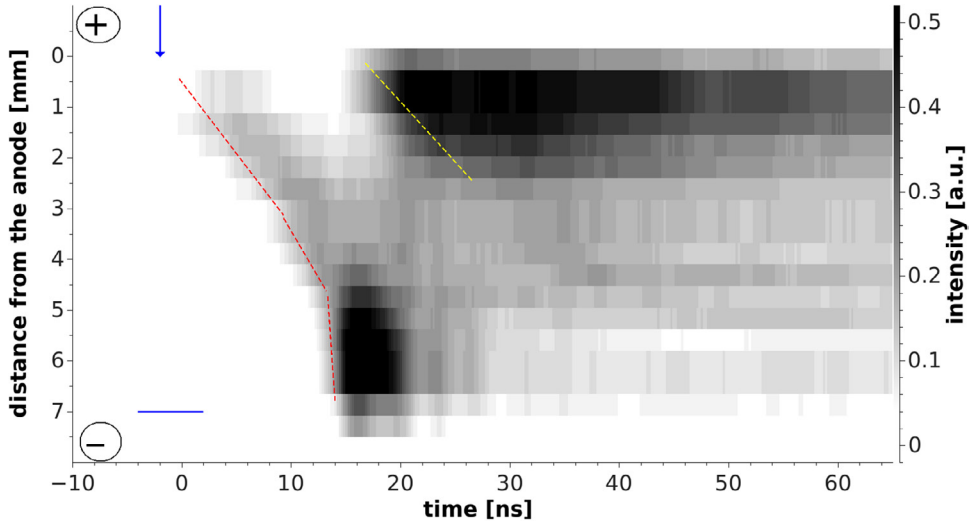

Figure 5. Visualization of the primary streamer and secondary streamer from spatio-temporal reconstruction of the PMT signals, $f \approx 1.5$ kHz, $d = 7$ mm, propagation path of the primary and the secondary streamer highlighted by the red and yellow dashed lines, respectively.

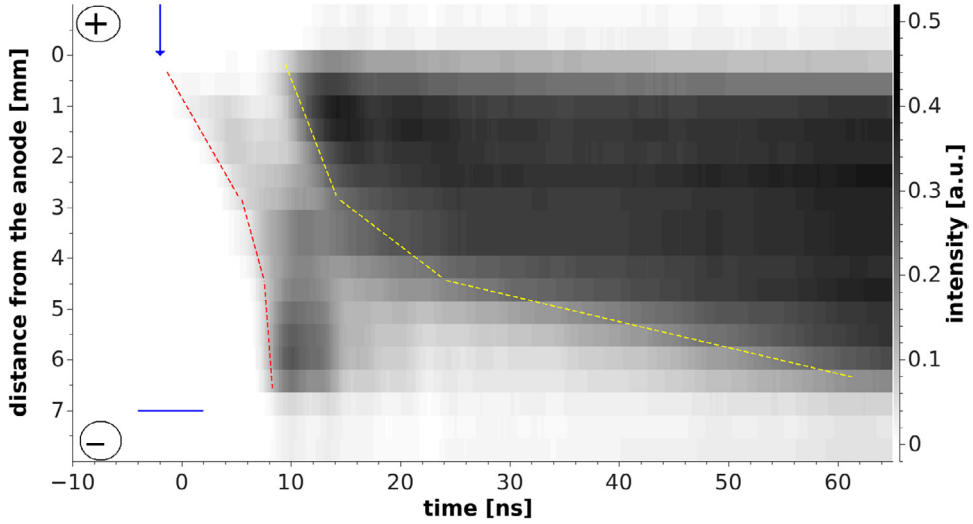

Figure 6. Visualization of the primary streamer and secondary streamer from spatio-temporal reconstruction of the PMT signals, $f \approx 6$ kHz, $d = 7$ mm, propagation path of the primary and the secondary streamer highlighted by the red and yellow dashed lines, respectively.

To keep the *E*/*N* above ~80 Td near the anode and even extend it towards the cathode, the decrease of *N* near the cathode is needed, as shown in the model of Bastien and Marode [14]. Without decrease of *N* near the cathode, the extension of the elevated *E*/*N* (>~80 Td) from the anode towards the cathode would not be possible. The extension of this 'high field' region would lead to the smoothening of the axial *E*/*N* distribution, with the average value below 80 Td. We previously estimated the average axial *E*/*N* in the plasma channel created by the primary streamer to be 60–70 Td [38], assuming no decrease of *N*. This means no additional generation of N_2(C) states and thus disappearance of the light emitting region (the secondary streamer) without its propagation through the whole gap. This corresponds to the actually observed situation in TS at frequencies below ~3 kHz (figure 5).

The decrease of *N* required for bridging the gap by the secondary streamer probably results from the heating of the gas inside the plasma channel created by the primary streamer, either via Joule heating or the two-step ultra-fast heating mechanism investigated by Rusterholtz *et al* [50], and Popov [51]. We assume that the heating and resulting decrease of *N* must be faster near the cathode to invoke the secondary streamer propagation. This is consistent with our results (figure 9); the gas heating, as indicated by the N_2(C) rotational temperature, was really faster near the cathode. It can be explained by higher densities of electrons and excited nitrogen molecules in this region. As a result, the elongation of the 'high field region' towards the cathode is accompanied by the propagation of the light emitting region (the secondary streamer) through the whole gap in TS at frequencies above ~3 kHz (figure 6). Although, the secondary streamer propagation velocity is slower during this 'propagation phase' compared to the initial 'formation phase', because it depends on the heating rate. At lower frequencies, where the heating rate and the temperature increase were slower (figure 10), the

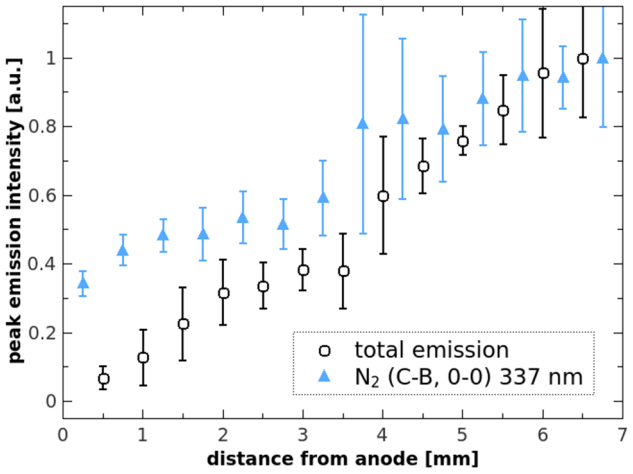

Figure 7. Normalized emission intensity of the primary streamer as it propagates through the gap as a function of the distance from the anode. Comparison of total emission with the emission at 337 nm filtered by the interference filter.

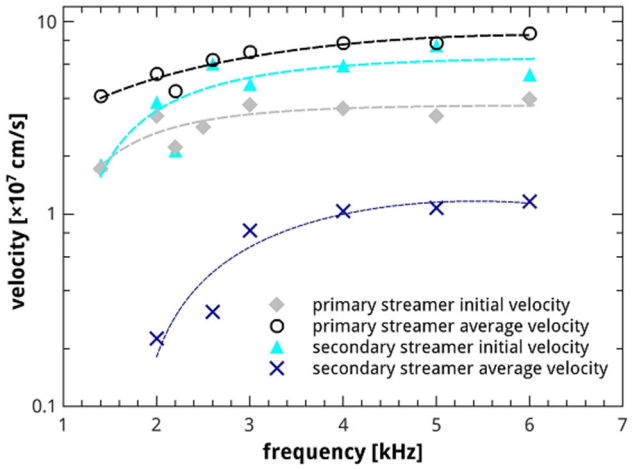

Figure 8. Primary and secondary streamer propagation velocities as functions of the TS repetition frequency.

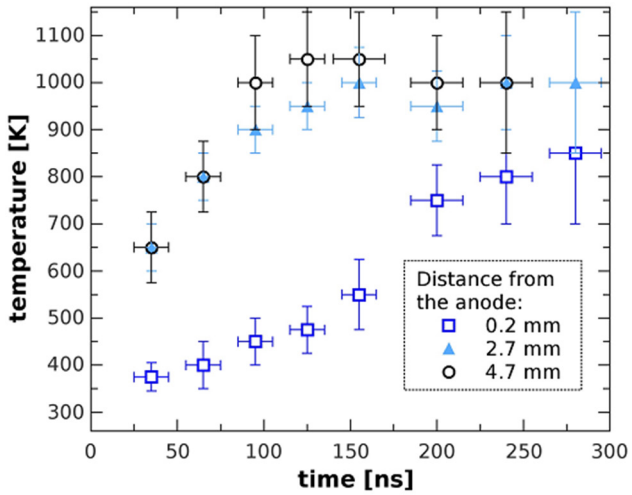

Figure 9. The N_2(C) rotational temperature evolution after the primary streamer at three different positions in the gap (near anode 0.2 mm, middle of the gap 2.7 mm, near cathode 4.7 mm), $f \approx 3.8$ kHz, $d = 5$ mm.

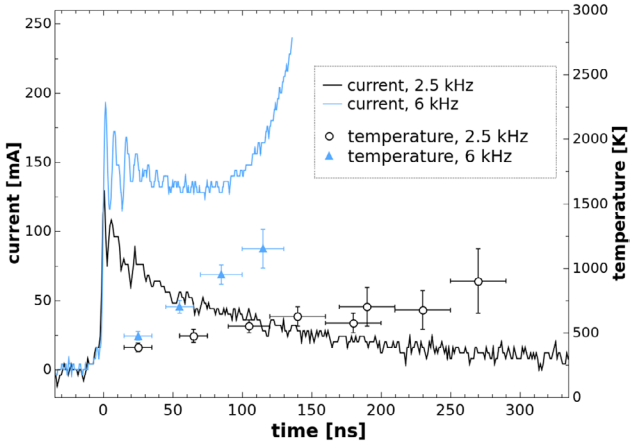

Figure 10. Temperature (measured at the anode) and current evolution as a function of time at different TS frequencies, $d = 5$ mm.

propagation of the secondary streamer towards the cathode was not observed at all.

The acceleration of the gas heating after the primary streamer with the increasing f could be explained by the electric current flowing through the generated plasma channel (Joule heating). The average current during the streamer-to-spark phase increases with the increasing f as illustrated in figure 10 and its evolution corresponds to the temperature evolution. At $f \sim 2.5$ kHz, the current after the streamer peak decreases quickly to a low value (~10 mA) and then remains low during the streamer-to-spark transition phase. On the other hand, at $f \sim 6$ kHz, the current drop after the streamer is much slower and after decreasing to ~130 mA, the current regrows towards the spark breakdown when the temperature exceeds ~1000 K. We have previously shown this temperature threshold of the streamer-to-spark breakdown [7].

The increase of TS repetition frequency leads to the gas heating (T_{str}, figure 3) and decrease of the initial N during the TS streamer phase. Lower N results in the lower attachment rate and slower decrease of electron density, i.e. slower decrease of the electric current during the streamer-to-spark transition phase. Furthermore, the changes in the treated gas composition caused by the previous TS pulses could also contribute to the decrease of the overall attachment rate. For example, the accumulation of atomic oxygen could increase the collisional detachment rate [52]. The accumulation of atomic O was also experimentally observed in nanosecond repetitively pulsed discharge at 10 kHz [53].

After the secondary streamer crosses the gap (time ~60 ns in figure 6), it takes a few more tens of ns before the actual spark appears. The delay between the moment when the secondary streamer reaches the cathode and the onset of the spark is probably because additional heating of the plasma channel is needed, up to previously reported ~1000 K [7]. Figure 9 supports this assumption, as the spark breakdown appears when temperatures near the cathode and anode equalize (time 250–300 ns in figure 9), i.e. the temperature near the anode also reaches ~1000 K. This suggests that the final step in the breakdown could be governed by the hydrodynamic expansion

mechanism suggested by Marode [13], leading to the increase of *E*/*N* in the core of the discharge channel and acceleration of the electron-impact ionization processes.

In addition, another explanation is also possible. We can expect further decrease of the net electron attachment rate due to acceleration of thermal collisional detachment reactions when the temperature increases up to ~1000 K. With very low attachment rate, the enhancement of *E*/*N* above ~80 Td along the gap thanks to the secondary streamer could be sufficient to increase the electron density and to initiate the spark breakdown. Even if 80 Td is not sufficient for efficient direct electron impact ionization of N_2 or O_2 molecules, it is certainly high enough to generate N_2(C) species observed as the secondary streamer, and also N_2(B) species with even lower excitation threshold energy. Next, the high density of excited N_2 molecules lead to the production and accumulation of species with lower ionization threshold energy, such as N_2(A) or NO. At higher TS frequencies, significant amount of nitrogen oxides can remain also from the previous TS pulses. This would enable efficient generation of new charged particles even at ~80 Td by chemical or step-wise ionization processes. The quantitative *in situ* measurements of NO and N_2(A) are needed to verify this hypothesis, but it is consistent with our previous results obtained at $f \approx 8$–10 kHz [36].

At $f \approx 8$–10 kHz, no decrease of the current after the primary streamer and almost instant transition to the spark was observed. Thanks to the high electron density (~10^{14} cm^{-3}), the stepwise ionization processes are assumed to play a significant role in the generation of electrons. With low attachment rate due to the memory effect (pre-heating and gas composition changes induced by the previous TS pulses), the stepwise ionization processes can form a positive feedback, as their importance increases with increasing electron density. Increasing electron density means higher plasma channel conductivity and faster discharging of internal capacity of the circuit, resulting to the spark current pulse formation.

At frequencies below ~3 kHz, the memory effect is much weaker and attachment rate is thus higher, leading to the fast decrease of current and electron density. As a result, the importance of stepwise ionization processes decreases in time and the breakdown mechanism is different, most probably based on the gas density decrease mechanism suggested by Marode [13], i.e. heating of the channel → increase of the pressure → hydrodynamic expansion → decrease of *N* in the core of the channel → increase of *E*/*N* → acceleration of ionization processes. For frequencies below ~3 kHz, a constriction of the discharge channel consistent with the simulations of Naidis [2] was observed [39], supporting this assumption.

4. Conclusions

We investigated the streamer-to-spark transition mechanism in the TS discharge in atmospheric pressure air at various pulse repetition frequencies (1–6 kHz). The TS is a self-pulsing discharge initiated by a primary streamer, with the subsequent short spark current pulse. The TS repetition frequency *f* can be controlled by the applied voltage. We succeeded to visualize the initial phases of the TS event: primary streamer and secondary streamer. The streak camera-like images were obtained from the set of optical emission intensity profiles measured by the PMT module along the inter-electrode gap. The signal from the PMT module was synchronized with the primary streamer current pulse.

The images of primary and secondary streamer propagation show that the spark breakdown mechanism in the TS changes with the increasing repetition frequency. In the TS, the increase of temperature up to ~1000 K was observed during the streamer-to-spark transition phase [39]. We therefore assume that the breakdown mechanism in the TS at frequencies below ~3 kHz is based on the gas density decrease suggested by Marode [13], i.e. heating of the channel → increase of the pressure → hydrodynamic expansion → decrease of *N* in the core of the channel → increase of *E*/*N* → acceleration of ionization processes. For $f > 3$ kHz, the breakdown mechanism is little different, and as our measurement showed, the secondary streamer plays an important role in it. The significant shortening of the streamer-to-spark transition time with the increasing TS repetition frequency can be actually explained by the fast heating of the gas between the electrodes and fast propagation of the secondary streamer through the whole gap.

The secondary streamer evolution is controlled by the rate of the gas heating created by the primary streamer in the plasma channel near the cathode. The accelerating gas heating resulting into higher propagation velocities of the secondary streamer with increasing *f* can be probably attributed to a memory effect—mostly to the pre-heating of the gas in the gap by the previous TS pulses. Due to the pre-heating, the gas density and thus also the electron attachment rate decrease with the increasing *f*. As a result, the electron density and electric current decrease only very slowly after the primary streamer at higher TS frequencies. Another memory effect, the accumulation of species such as oxygen atoms generated by previous TS pulses can also lead to the decrease of the electron attachment rate. With low attachment rate, the production of electrons by stepwise ionization processes and a weak direct electron impact ionization in the secondary streamer are probably sufficient to initiate spark transition even without the increase of *E*/*N*. Further research is however required, including kinetic modeling and measurements of ground state O atoms density, to verify this hypothesis.

Acknowledgments

Effort sponsored by the Slovak Research and Development Agency APVV-0134-12, and Slovak grant agency VEGA 1/0918/15. This publication is also the result of the project implementation: ITMS codes 26240220042, supported by the Research & Development Operational Programme funded by the European Regional Development Fund (ERDF).

References

[1] Larsson A 1998 *J. Phys. D: Appl. Phys.* **31** 1100
[2] Naidis G V 2009 *Eur. Phys. J. Appl. Phys.* **47** 22803
[3] Pai D Z, Lacoste D A and Laux C O 2010 *Plasma Sources Sci. Technol.* **19** 065015
[4] Pai D Z, Lacoste D A and Laux C O 2010 *J. Appl. Phys.* **107** 093303
[5] Gerling T, Hoder T, Brandenburg R, Bussiahn R and Weltmann K-D 2013 *J. Phys. D: Appl. Phys.* **46** 145205
[6] Peek F W Jr 1929 *Phenomena in High Voltage Engineering* (New York: McGraw-Hill)
[7] Llewellyn-Jones F 1966 *Ionization and Breakdown in Gases* (London: Methuen)
[8] Meek M J and Craggs J D 1978 *Electrical Breakdown of Gases* (New York: Wiley)
[9] Meek J M 1940 *Phys. Rev.* **57** 722
[10] Raether H 1964 *Electron Avalanches and Breakdown in Gases* (London: Butterworths)
[11] Loeb L B 1965 *Electrical Coronas* (Berkeley, CA: University of California Press)
[12] Marode E 1975 *J. Appl. Phys.* **46** 2005
[13] Marode E, Bastien F and Bakker M 1979 *J. Appl. Phys.* **50** 141
[14] Bastien F and Marode E 1985 *J. Phys. D: Appl. Phys.* **18** 377
[15] Morrow R and Lowke J J 1997 *J. Phys. D: Appl. Phys.* **30** 614
[16] Aleksandrov N L and Bazelyan E M 1999 *Plasma Sources Sci. Technol.* **8** 285
[17] Kulikovsky A A 2001 *IEEE Trans. Plasma Sci.* **29** 313
[18] Bourdon A, Bonaventura Z and Celestine S 2010 *Plasma Sources Sci. Technol.* **19** 034012
[19] Šimek M 2014 *J. Phys. D: Appl. Phys.* **47** 463001
[20] Pai D Z, Stancu G D, Lacoste D A and Laux C O 2009 *Plasma Sources Sci. Technol.* **18** 045030
[21] Mihaila I, Ursu C, Gegiuc A and Popa G 2010 *J. Phys.: Conf. Ser.* **207** 012005
[22] Le Delliou P, Tardiveau P, Jeanney P, Bauville G and Pasquiers S 2011 *IEEE Trans. Plasma Sci.* **39** 2686
[23] Bentaleb S, Tardiveau P, Moreau N, Jeanney P, Jorand F and Pasquiers S 2011 *IEEE Trans. Plasma Sci.* **39** 2236
[24] Kettlitz M, Hoeft H, Hoder T, Reuter S, Weltmann K-D and Brandenburg R 2012 *J. Phys. D: Appl. Phys.* **45** 245201
[25] Grosch H, Hoder T, Weltmann K-D and Brandenburg R 2010 *Eur. Phys. J.* D **60** 547–53
[26] Šimek M, Ambrico P F and Prukner V 2011 *Plasma Sources Sci. Technol.* **20** 025010
[27] Hoder T, Wilke C, Loffhagen D and Brandenburg R 2011 *IEEE Trans. Plasma Sci.* **39** 2158
[28] Laux O, Spence T G, Kruger C H and Zare R N 2003 *Plasma Sources Sci. Technol.* **12** 125
[29] Fantz U 2006 *Plasma Sources Sci. Technol.* **15** S137
[30] Marode E, Samson S, Djermoune D, Deschamps N, Touzeau M and De Souza R 1999 *J. Adv. Oxid. Technol.* **4** 305–11
[31] Ivkovic M, Jovicevic S and Konjevic N 2004 *Spectrochim. Acta* B **59** 591
[32] Jánský J, Le Delliou P, Tholin F, Bonaventura Z, Tardiveau P, Bourdon A and Pasquiers S 2011 *IEEE Trans. Plasma Sci.* **39** 2106
[33] Brandenburg R, Hoder T and Wagner H-E 2008 *IEEE Trans. Plasma Sci.* **36** 1318
[34] Hoder T, Cernak M, Paillol J, Loffhagen D and Brandenburg R 2012 *Phys. Rev.* E **86** 055401
[35] Brandenburg R *et al* 2013 *J. Phys. D: Appl. Phys.* **46** 464015
[36] Janda M, Hoder T, Sarani A, Brandenburg R and Machala Z 2017 *Plasma Sources Sci. Technol.* **26** 055010
[37] Marode E, Goldman A and Goldman M 2011 High pressure discharge as a trigger for pollution control *Non-Thermal Plasma Techniques for Pollution Control (NATO ASI series, Part A)* (Berlin: Springer) pp 167–90
[38] Janda M, Martišovitš V and Machala Z 2011 *Plasma Sources Sci. Technol.* **20** 035015
[39] Janda M, Machala Z, Niklová A and Martišovitš V 2012 *Plasma Sources Sci. Technol.* **21** 045006
[40] Janda M, Martišovitš V, Hensel K, Dvonc L and Machala Z 2014 *Plasma Sources Sci. Technol.* **23** 065016
[41] Machala Z, Chládeková L and Pelach M 2010 *J. Phys. D: Appl. Phys.* **43** 222001
[42] Machala Z, Tarabová B, Hensel K, Špetlíková E, Šikurová L and Lukeš P 2013 *Plasma Process. Polym.* **10** 649
[43] Hontanon E, Palomares J M, Stein M, Guo X A, Engeln R, Nirschl H and Kruis F E 2013 *J. Nanopart. Res.* **15** 1957
[44] Machala Z, Janda M, Hensel K, Jedlovský I, Leštinská L, Foltin V, Martišovitš V and Morvová M 2007 *J. Mol. Spectrosc.* **243** 194
[45] Gerling T, Hoder T, Bussiahn R, Brandenburg R and Weltmann K-D 2013 *Plasma Sources Sci. Technol.* **22** 065012
[46] Sigmond S R 1984 *J. Appl. Phys.* **56** 1355
[47] Marode E *et al* 2009 *Plasma Phys. Control. Fusion* **51** 124002
[48] Ono R and Oda T 2007 *J. Phys. D: Appl. Phys.* **40** 176
[49] Hoder T, Bonaventura Z, Bourdon A and Simek M 2015 *J. Appl. Phys.* **117** 073302
[50] Rusterholtz L, Lacoste D A, Stancu G D, Pai D Z and Laux C O 2013 *J. Phys. D: Appl. Phys.* **46** 464010
[51] Popov N A 2011 *J. Phys. D: Appl. Phys.* **44** 285201
[52] Janda M, Machala Z, Dvonc L, Lacoste D A and Laux C O 2015 *J. Phys. D: Appl. Phys.* **48** 035201
[53] Stancu G D, Kaddouri F, Lacoste D A and Laux C O 2010 *J. Phys. D: Appl. Phys.* **43** 124002